MAGNETIC RESONANCE IN MEDICINE **16**, 317–334 (1990)

Nuclear Relaxation of Human Brain Gray and White Matter: Analysis of Field Dependence and Implications for MRI

HELMUT W. FISCHER,*† PETER A. RINCK,‡ YVES VAN HAVERBEKE,* AND ROBERT N. MULLER*,[1]

*University of Mons, Department of Organic Chemistry and NMR Laboratory, Medical Faculty, B-7000 Mons, Belgium; †University of Bremen, Department of Physics, D-2800 Bremen 33, Federal Republic of Germany; and ‡MR Center, Medical Section, N-7006 Trondheim, Norway

Received June 12, 1989; revised November 20, 1989

The dependence of $1/T_1$ on the magnetic field strength (the relaxation dispersion) has been measured at 37°C on autopsy samples of human brain gray and white matter at field strengths corresponding to proton Larmor frequencies between 10 kHz and 50 MHz (0.0002–1.2 T). Additional measurements of $1/T_1$ and $1/T_2$ have been performed at 200 MHz (4.7 T) and 20 MHz (0.47 T), respectively. Absolute signal amplitudes are found to be proportional to the sample water content, not to the "proton density," and it is concluded that the myelin lipids do not contribute to the signal. Transverse magnetization decay data can be fitted with a triple exponential function, giving characteristic results for each tissue type, and are insensitive to variations of the pulse spacing interval. The longitudinal relaxation dispersion curves show characteristic shapes for each tissue type. The most striking difference is a large dispersion for white matter at very high fields. As a consequence, the relative difference in $1/T_1$ between gray and white matter shows a marked maximum around 10 MHz. Possible implications for MRI are discussed. A weighted least-squares fit of the dispersions has been performed using a four-parameter function of the form

$$1/T_1 = 1/T_{1,w} + D + A/(1+(f/f_c)^{\beta'}).$$

The quality of the fit is superior to that of other functions proposed previously. The results of these fits are used to predict image contrast between gray and white matter at different field strengths.

INTRODUCTION

Whereas in the beginning of medical NMR the dependence of the nuclear relaxation times, especially T_1, on the magnetic field strength was often overlooked, nowadays it is a well-known fact of recognized importance. The main consequence for the researcher involved in imaging is negative: first, the comparison of results obtained at different field strengths is often difficult, unless the form of the T_1 dispersion is known, and second, the increase of the longitudinal relaxation time of almost all biological materials with field makes longer repetition times necessary at higher fields, partially counteracting the desired increase in signal-to-noise ratio.

On the other hand, it is often ignored that the analysis of the field dependence of

[1] To whom correspondence should be addressed.

0740-3194/90 $3.00

the relaxation time T_1 or relaxation rate $1/T_1$ can give valuable information at the molecular level about the structure and dynamics of the system under investigation. Since experiments of this kind are preferably performed *in vitro* and with specialized instrumentation, the effect of tissue excision and storage must, of course, be thoroughly investigated. This has been done in a previous study (*1*).

Imaging of the central nervous system (CNS) is nowadays one of the most important applications of medical NMR. The original aim of the present study, which concentrates on normal human brain tissues, was to develop reproducible standard longitudinal relaxation dispersions of the most important tissues, namely gray and white matter, combined with the other relevant NMR parameters $1/T_2$ and ρ (the proton density), in order to allow the prediction of image contrast for given instrumentation characteristics and imaging sequence and settings. The long-term aim is to produce similar data for the most important pathologies. This will offer the possibility to derive optimal search strategies for a given diagnostical need and to optimize the imaging parameters for such a purpose.

Another aim is a mathematical analysis of the obtained data by curve fitting and parameter extraction. On the one hand, this approach allows the interpolation for field strengths not investigated experimentally, and on the other hand, using a suitable function, the obtained parameters can be compared with predictions from biophysical theories and models.

Throughout this text, the term "relaxation rate" (meaning $1/T_1$ or $1/T_2$) is used instead of the more common "relaxation time." The reason lies in the well-known fact that for different relaxation processes sensed by the same spin system, the relaxation rates are additive and thus the plot of the relaxation rate vs another parameter can be very illustrative and eventually allows the identification of the different underlying processes.

EXPERIMENTAL

Sample Preparation

Normal human brain gray and white matter samples from various anatomical locations of the brain were excised, within 24 h after death, from patients who died of other than neurological causes. Tissue samples weighing between 200 and 600 mg were transferred to 75-mm-long, 10-mm-o.d. sample tubes directly after dissection, quickly deep frozen on dry ice (−78.5°C), transported to the NMR laboratory on dry ice, and stored in a deep freezer until examination. The samples were thawed at room temperature 10 to 20 min before the beginning of the measurements and were then allowed to reach thermal equilibrium in the warm probehead for about 5 min. Previous experiments on rat brain tissues have shown that the storage procedure does not significantly affect the nuclear relaxation properties of normal brain tissues (*1*). Similarly, Györffy-Wagner *et al.* found no change in $1/T_1$ and a very slow increase of $1/T_2$ with time (about 10% within 90 h) for pork brain tissues stored at 8°C and measured at 37°C and 10.7 MHz (*2*).

For additional measurements, one or several pieces of tissue were taken out of the sample tube by aspiring with a plastic straw and transferred to 150-mm-long, 7-mm-o.d. tubes. The maximum weight of these samples was 200 mg. Samples were stored

at 7°C between measurements, and all the measurements were performed within 24 h after thawing of the samples.

NMR Measurements

The longitudinal proton relaxation dispersion was recorded with an IBM research relaxometer, a field cycling machine of which the detailed description has been published recently (*3*). On this system, $1/T_1$ can be measured at any magnetic field strength between 0.00024 and 1.2 T, corresponding to Larmor frequencies between 0.01 and 50 MHz. A typical experiment consisted of recording 10 to 15 $1/T_1$ values and lasted between 30 and 60 min. Normally, for each $1/T_1$ measurement, 15 points along the magnetization evolution were recorded over a time period covering 1.5 times the estimated T_1, accompanied by 8 "infinity" points at 7 times the estimated T_1. The experimental error in the $1/T_1$ determination was between 1 and 2%. As the signal is recorded using a spin–echo sequence with an echo delay time of $2\tau = 6$ ms, only the "liquid" part of the NMR signal is measured. Additional data were obtained on conventional pulse spectrometers (Bruker MSL 200-15 and Bruker Minispec PC 20): $1/T_1$ at 4.7 T by inversion-recovery (about 10 points) and $1/T_2$ at 0.47 T by CPMG (500 to 1500 echoes, of which every 10th was digitized) pulse sequences, respectively. In one case, a high-resolution spectrum of a white matter sample was obtained on the 200-MHz machine. All NMR data were recorded at a sample temperature of 37°C. Water content was determined by drying the tissues for at least 7 days at 70°C. Lipid content was determined by petroleum ether extraction as described by Beall *et al.* (*4*).

Data Analysis

The longitudinal relaxation dispersion data were submitted to a weighted least-squares curve-fitting procedure. The function used (*5, 6*) is similar to the "Cole–Cole Fit" used in dielectric relaxation and successfully applied to NMR relaxation dispersion data of protein solutions (*7, 8*) and tissues (*9, 10*),

$$\frac{1}{T_1} = \frac{1}{T_{1,w}} + D + \frac{A}{1 + (f/f_c)^{\beta'}} \qquad [1]$$

where f = Larmor frequency in MHz, $1/T_{1,w}$ = relaxation rate of pure water (0.23 s^{-1} at 37°C), D = baseline, A = height of dispersion step, f_c = inflection frequency, and β' = steepness of the dispersion step. The value for $1/T_{1,w}$ has been determined previously on oxygen-free water in the Minispec.

The Cole–Cole function as used in (*7–10*) has the form

$$\frac{1}{T_1} = \frac{1}{T_{1,w}} + D + \frac{A(1+(f/f_c)^{\beta/2}\cos(\pi\beta/4))}{1 + 2(f/f_c)^{\beta/2}\cos(\pi\beta/4) + (f/f_c)^{\beta}} \qquad [2]$$

with the parameters defined as in Eq. [1]. For $\beta' = 2$ resp. $\beta = 2$ the form of both curves is the same and is identical to a Lorentzian dispersion. For broader dispersions, as encountered with protein solutions or tissues, both curves have a very similar shape, and parameters from both fits, when applied to the same set of data, within the error

limits give the same results, except for the exponent. Here, β' is always lower than β. The only reason for using Eq. [1] instead of Eq. [2] is its mathematical simplicity, making its use more convenient. The quality of the fit obtained with both functions, judged by the χ^2 resulting from the fit procedure (see below), is identical. When applied to protein solution data, Eq. [2] has been proven to give results with biophysical meaning (*7, 8*): D and A are proportional to the solute concentration, and f_c is proportional to the inverse of the rotational correlation time of the protein, τ_c. Although these findings cannot be transferred directly to such complex systems as tissues, one can consider tissues as protein solutions in a first approach. So one could expect to find, e.g., a higher value for parameter A on tissues with low water content or parameter β' to reflect the width of the distributions of relaxation-effective molecular processes with different time scales. Parameters obtained with Eq. [1] or Eq. [2] on tissue data can thus be of biophysical value and are potentially useful for tissue characterization (*11*).

Bottomley *et al.* (*12, 13*) have applied a now widely used two-parameter function of the form

$$T_1 = Af^B \qquad [3]$$

to tissue data collected from the literature and obtained between 1 and 100 MHz. This function tends toward zero at low fields and toward very high values at high fields. A modification of Eq. [3] with two additional parameters for the physically plausible and experimentally encountered low-field (L) and high-field (H) limits could have the form

$$\frac{1}{T_1} = H + \frac{1}{A(f^B + L)}, \qquad [4]$$

which is mathematically equivalent to Eq. [1]. In its original form, Eq. [3] is not suitable for application to our data, as it reveals neither the inflection point nor the high-field plateau. If Eq. [3] is applied to our data restricted to the range 1–200 MHz, the fit is better and the parameters are quite similar to those obtained in (*12, 13*). However, the quality of the fit using Eq. [1] is still superior, as is shown below.

The numerical procedure was performed using the iterative program package MINUIT developed at CERN (*14*). After the input of relaxation dispersion data pairs (frequency and relaxation rate, plus the standard deviation of the latter) the analysis of a typical relaxation dispersion as described above produces values for the parameters, their standard deviation, and χ^2. The χ^2 was also the function to be minimized and according to which the quality of the fit was assessed.

Some of the transverse magnetization decay data were analyzed for multiexponentiality by least-squares fitting using the same program package. The quality of the fit was judged according to the χ_2, its variation with the number of parameters, and the distribution of the residuals (*15*).

RESULTS

Signal Height and Tissue Water Content

In order to decide to what extent the myelin lipids, which are abundant in white matter (55% dry weight or 16% wet weight (*16*)), contribute to the liquid NMR signal,

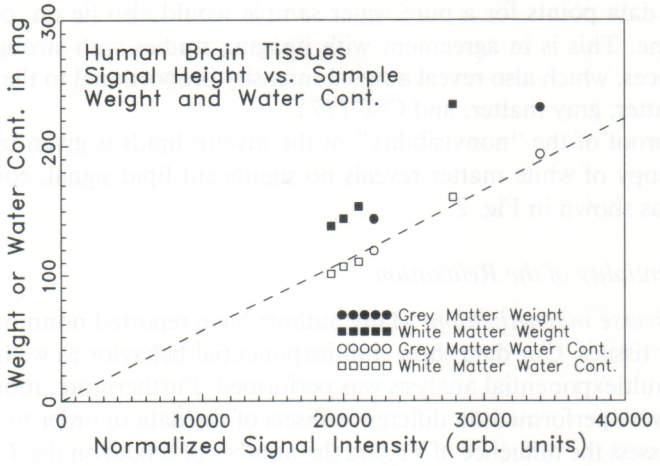

FIG. 1. Sample weight and water content plotted versus the normalized signal intensity (M_0 extrapolated from the transverse decay data, divided by the receiver attenuation factor) for various gray and white matter samples from the same individual at 0.47 T. The dashed line represents the regression for the water content data ($R^2 = 0.976$), proving the proportionality between signal and water content.

sample weights and water contents were plotted against the normalized signal amplitude (i.e., the digitized signal amplitude divided by the receiver attenuation factor). The data used were taken from CPMG pulse trains with small interpulse delay ($2\tau = 230$ μs, 1500 echoes, every 10th echo digitized). To exclude T_2 effects on the signal height, the initial magnetization M_0 was calculated from a triple exponential fit, as described below. The results obtained on M_0 are shown in Fig. 1.

It is clear that gray and white matter give different signal/weight ratios, and that both data sets are united when the water content is considered instead of the total

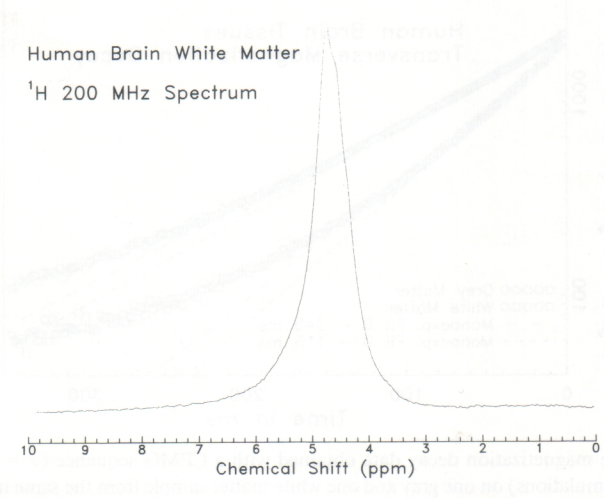

FIG. 2. Proton spectrum of a white matter sample, obtained at 200 MHz. No lipid signal (around 1.2 ppm) is observed.

weight. The data points for a pure water sample would also lie on, or close to, the regression line. This is in agreement with imaging studies with strongly ρ-weighted pulse sequences, which also reveal a signal intensity proportional to the water content for white matter, gray matter, and CSF (*17*).

Another proof of the "nonvisibility" of the myelin lipids is given by the fact that ^{1}H spectroscopy of white matter reveals no significant lipid signal, compared to the water peak, as shown in Fig. 2.

Multiexponentiality of the Relaxation

(a) Transverse magnetization. Many authors have reported nonmonoexponential T_2 decay for tissues. Our data show multiexponential behavior as well, and on some data sets a multiexponential analysis was performed. Furthermore, monoexponential regressions were performed on different subsets of the data in order to simulate MRI data and to assess the influence of TE and the number of echoes on the T measurement.

Figure 3 shows transverse magnetization data for one sample of gray and white matter; the deviation from a single exponential can be clearly seen. Also visible is the more pronounced deviation for white matter than for gray matter. This fact is also reflected by the multiexponential analysis: the quality of the fit increased only slightly for gray matter when the number of components was increased from two to three, whereas the change was marked for white matter. Fitting with more than three components gave no significant improvement in the fit for either of the tissue data sets. Results from the analysis are presented in Table 1. At this stage of our work, no further interpretation of the extracted parameters, e.g., in terms of bound, intra-, and extracellular water (*15, 18*), is given.

The data in Table 1, in accordance with literature data (*19, 20*), show a large difference in $1/T_2$ between gray and white matter for the monoexponential fit, when

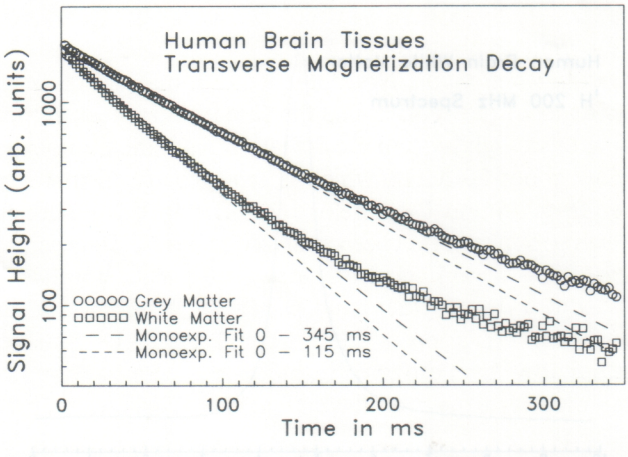

FIG. 3. Transverse magnetization decay data obtained with a CPMG sequence (τ = 115 μs, every 10th echo digitized, 9 accumulations) on one gray and one white matter sample from the same individual (location, temporal) at 0.47 T. The dashed lines represent monoexponential least-squares fits to all data points (long dashes) and to the data up to t = 115 ms (short dashes). For numerical results see Table 1.

TABLE 1

Results of a Multiexponential Analysis of the Transverse Magnetization Decay Data Shown in Fig. 1

	White matter		Gray matter	
Number of components	Ampl. (%)	$1/T_2$ (s^{-1})	Ampl. (%)	$1/T_2$ (s^{-1})
1	9.8	79.4	3.5	93.5
2	83.4	17.0	91.0	9.8
3	6.8	2.39	5.4	1.21
Monoexp. fit, 0–345 ms		14.47		9.44
Monoexp. fit, 0–115 ms		16.03		10.24

compared to results reported in most imaging studies. There the difference is often around 20%. This finding can in part be attributed to the sampling interval, which is much larger in imaging studies and thus excludes the fast component, which is more pronounced for white matter, as can be seen in Table 1. Accordingly, the difference in $1/T_2$ decreases when only every 10th or 20th data point is used for the regression analysis. Another reason for the smaller difference found in imaging studies might be due to partial volume effects, predominantly in gray matter.

From these results we can only stress once again the care which must be taken in interpreting T_2 data of tissues, as the results depend on the measurement and regression techniques. On the other hand, a single exponential, produced by a small number of points, may be sufficient to describe the behavior of the transverse magnetization with time, as the absolute deviation of such a curve from the true magnetization values is rather small, i.e., below 5% in most cases.

For further use in this study, $1/T_2$ data resulting from 50 data points recorded over a time interval of 115 ms (the standard protocol of our experiments) have been used. In this way, the best fit to the first part of the echo train ($TE \leqslant 1.5T_2$), which is the most important for comparison with MRI results, is obtained.

(b) Longitudinal magnetization. Normally, longitudinal relaxation of tissues is reported to be monoexponential. This is also the case for our measurements. However, for white matter we see a slight systematic deviation from the monoexponential function, at fields below about 20 MHz, which is reflected by an increase in the $1/T_1$ standard deviation from around 1% at fields >20 MHz to 1.5–2% at fields <20 MHz. The origin of this behavior has not yet been analyzed in detail. However, as the deviation from a single exponential is very small, the latter still gives a good description of the magnetization evolution. On the other hand, the (field-dependent) deviation from the single exponential is an indication of an additional fact to be considered when the relaxation in white matter is investigated in more detail. Preliminary results indicate a small slow component present at all field strengths.

Effects of the Interpulse Delay on $1/T_2$ Measurements

Several authors have observed different evolutions of the transverse magnetization of tissues, when the interpulse delay τ was varied in CPMG experiments (*21, 22*).

This effect was attributed to relaxation in the rotating frame (*21*) and to chemical exchange (*22*). In order to obtain an estimate of possible influences of the short τ normally used in our experiments, τ was varied in one experiment. The result is shown in Fig. 4. The graph proves that in our experimental setup, no dependence of the transverse magnetization decay on τ is observable, when 2τ is varied between 230 and 2300 μs. Even the shortest τ is probably long enough to exclude $T_{1\rho}$ effects (*21*). On the other hand, the increase of $1/T_2$ with increasing τ, as observed in (*21*) in brain tissues (about 20% when 2τ is varied from 200 to 2000 μs), could not be reproduced here, although the same instrumentation was used.

Longitudinal Relaxation Dispersions

A typical relaxation dispersion for two samples of gray and white matter is shown in Fig. 5 and Table 2. It can be seen that the curves exhibit clearly different shapes. The dispersion for white matter is much more pronounced at high fields, and the relaxation rate is generally higher. The latter fact is well known, and the former has been reported recently (*11, 23*). Furthermore, according to our investigations of a variety of human and animal tissues, this high-field dispersion is a charcteristic unique to white matter (*11*). All other tissues show dispersions which are almost flat (i.e., very little change in $1/T_1$ with field) at high fields. The only exception is adipose tissue (cf. (*1, 10, 24*)). However, the relaxation mechanism for this tissue is completely different from those of other tissues due to its different chemical composition and structure. The NMR signal of fat originates mainly from the aliphatic protons of the triglycerides, whereas for other tissues the signal comes from the tissue water. Due to their high transverse relaxation rate $1/T_2$ ($>1000\ s^{-1}$), the polar lipids, though abundant in white matter, do not contribute to the liquid signal observed in our relaxometry experiments and in MRI sequences. This leads to a NMR signal height which is proportional to the water content of the tissue, but not to the proton desnity, as shown in the previous paragraph. In accordance with these considerations, the water content

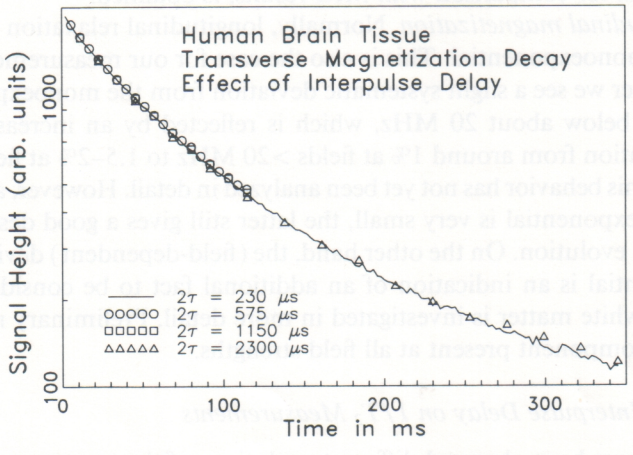

FIG. 4. CPMG echo trains obtained on the same sample (white matter) with various interpulse delays. No systematic variations in the decay can be observed.

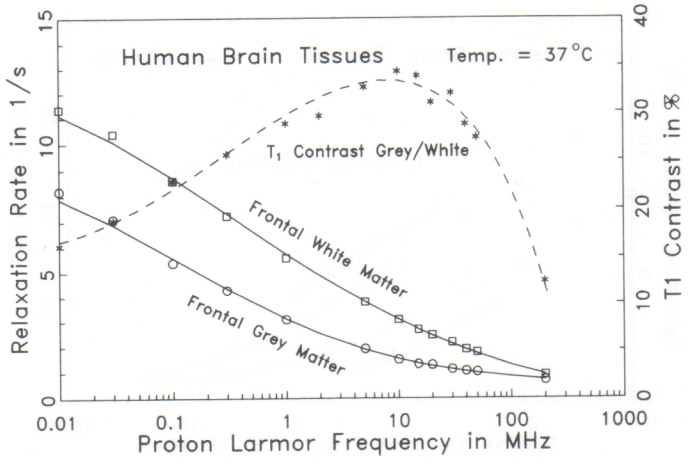

FIG. 5. Longitudinal relaxation dispersions of frontal gray and white matter from the same brain. Also displayed is the T_1 contrast obtained with Eq. [5]. The solid lines through the data points are the result of numerical curve fitting using Eq. [1]; the dashed curve through the T_1 contrast points is obtained by applying Eq. [5] to the fitted $1/T_1$ data points. The fit parameters are given in Table 2.

of the tissues as given in Table 2 agrees very well with data on "proton density" obtained by MRI in long-TR sequences, resulting in 0.72 for white matter and 0.84 for gray matter, relative to 1 for CSF (*17*).

It can also be seen from Table 2 that all fitted parameters differ significantly for both tissues. However, for white matter a negative baseline (parameter D) is obtained, reducing the physical plausibility of the fit model.

Also displayed in Fig. 5 is the "T_1 contrast" obtained with the formula

$$C_{T_1} = |(1/T_{1,A} - 1/T_{1,B})|/(1/T_{1,A} + 1/T_{1,B}). \quad [5]$$

This "object contrast" is a measure of the relative difference of the relaxation rates (or relaxation times) of two tissues at a given field strength and can be of use to assess the possibility of discriminating between two tissues at different fields, i.e., the image

TABLE 2

Fit Parameter Values and Additional Data for Two White/Gray Matter Samples from the Same Region of the Same Brain, as Shown in Fig. 5 ($T_{1,w} = 0.23\ s^{-1}$)

Parameter	White matter	Gray matter
D (s^{-1})	−1.38	0.105
A (s^{-1})	18.25	11.66
f_c (MHz)	0.165	0.059
β'	0.291	0.42
$1/T_2$ (s^{-1})	17.21	9.63
Water content (%)	71.5	84.0
Lipid content (%)	17.0	5.4

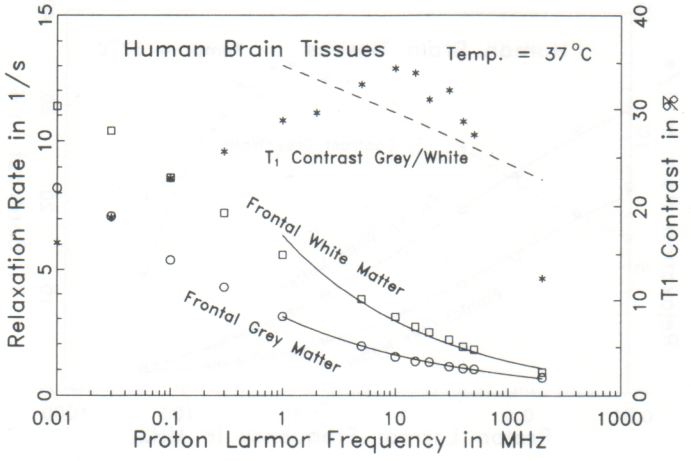

FIG. 6. Same data as in Fig. 5; the solid lines represent the best fit to the data between 1 and 200 MHz using Eq. [3]. The fit parameters are given in Table 3. The dashed line is the T_1 contrast as it would result from the fit curves.

contrast. Here it is obvious that, due to the "abnormal" dispersion of white matter, the T_1 contrast curve has a maximum at medium fields around 10 MHz. The same behavior is observed when white matter is compared to other tissues like tumors, which also lack the high-field component in their dispersion profiles. Possible implications of this finding for MRI have been addressed in previous papers (*24*, *25*) and some new aspects are discussed below.

The dashed line is calculated from the fit curves for the two tissues. As the plot of differences is very sensitive to deviations between data and calculated values, the excellent fitting of the contrast curve is a proof of the quality of the fit model, not obtained with any other formula which has been tested, such as Eq. [3] or the function $1/T_1 = Af^{1/2} + B$, as proposed by Escanye *et al.* (*26*). For comparison, the fit curves and the resulting calculated T_1 contrast curve using Eq. [3] for the data between 1 and 200 MHz are displayed in Fig. 6, and the resulting fit parameters are shown in Table 3.

TABLE 3

Fit Parameters Obtained with Eq. [3], When Applied to the Data in Fig. 6, Limited to 1 MHz $\leqslant f \leqslant$ 200 MHz

	White matter		Gray matter	
Parameter	This work	Ref. (*12*)	This work	Ref. (*12*)
A	0.00144	0.00152	0.00587	0.00362
B	0.3397	0.3477	0.2903	0.3082

Note. The data obtained by Bottomley *et al.* (*12*) for brain white and gray matter using the same formula are displayed for comparison. The differences in parameter A for gray matter are most probably due to partial-volume effects in MRI experiments.

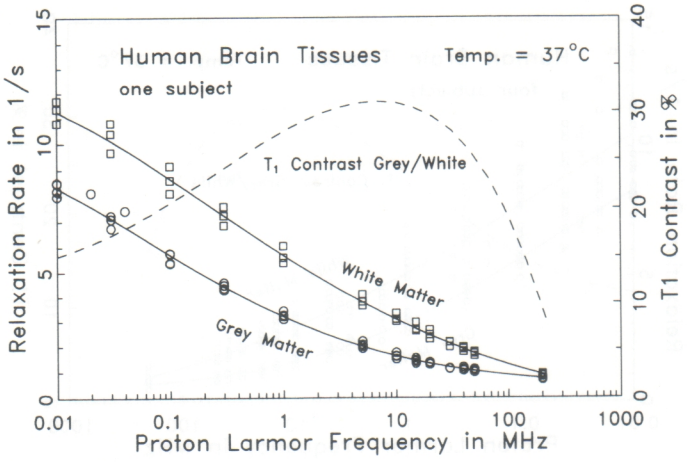

FIG. 7. Joint treatment of all white and gray matter samples from one brain. The fit parameters are given in Table 4.

It can clearly be seen that the inferior quality of the fit, especially for white matter, leads to an unsatisfying result for the fit of the T_1 contrast data (which for mathematical reasons has to be a straight line in this type of graphic representation). This finding contradicts (for the data used here) the statement made in (*12*) that Eq. [3] gives equivalent or even better fits to individual tissue dispersions than Eq. [2].

For samples from different regions in the brain or from different patients, biological variability comes into play. Figure 7 and Table 4 show the data for all homogeneous samples from one subject, from different regions of the brain (frontal, temporal and parietal white and gray matter plus cerebellar gray matter). The fit parameters were obtained by procesing all data points simultaneously, whereas $1/T_2$, water content, and lipid content are averages over the individual values.

It can be seen that the scattering of the data points is rather low. The fit parameters

TABLE 4

Fit Parameter Values for a Joint Treatment of Three White Matter and Four Gray Matter Samples from One Brain, as Shown in Fig. 7

Parameter	White matter	Gray matter
D (s^{-1})	−1.06	0.13
A (s^{-1})	15.97	11.21
f_c (MHz)	0.32	0.081
β'	0.328	0.428
$1/T_2$ (s^{-1})	16.90 ± 0.77	9.67 ± 0.51
Water content (%)	72.0 ± 1.4	84.0 ± 0.8
Lipid content (%)	16.3 ± 1.0	4.2 ± 1.3

Note. $1/T_2$, water content and lipid content are averages; the corresponding standard error is indicated. $T_{1,w} = 0.23$ s^{-1}.

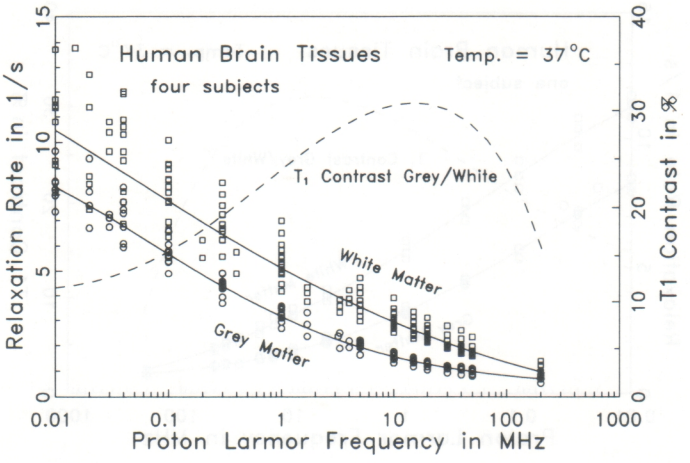

FIG. 8. Joint treatment of all white and gray matter samples from four different brains. The fit parameters are given in Table 5.

did not undergo significant changes and the T_1 contrast curve, calculated from the two fit curves, maintained the same shape.

The same holds for a joint treatment of all our data, stemming from 10 samples of gray matter and 13 samples of white matter from four different individuals, as shown in Fig. 8 and Table 5.

In spite of the larger scattering of the data due to interindividual variability, the two groups are clearly separated at medium fields, where the T_1 contrast is maximal, whereas they overlap at high and low fields. The tissue dispersions and the resulting T_1 contrast curve again have the characteristic shape.

Regional differences in relaxation properties of tissue samples within the same brain, as observed by other authors (*20*), were not found in this study. The difference in $1/T_1$ and $1/T_2$ between, e.g., frontal and parietal gray matter, appeared random when

TABLE 5

Fit Parameter Values for a Joint Treatment of 13 White Matter and 10 Gray Matter Samples from Four Different Brains, as Shown in Fig. 8

Parameter	White matter	Gray matter
D (s^{-1})	−1.52	0.11
A (s^{-1})	19.07	11.08
f_c (MHz)	0.067	0.085
β'	0.251	0.438
$1/T_2$ (s^{-1})	16.14 ± 2.85	9.64 ± 0.84
Water content (%)	71.6 ± 2.6	83.7 ± 1.8

Note. $1/T_2$ and water content are averages from 8 white matter and 7 gray matter samples. $T_{1,w} = 0.23\ s^{-1}$.

data from several brains were compared. However, the differences found in (*20*) were on the order of 10 to 20%, little larger than the sample standard deviation, and became significant only given a large number of samples (>100), which is not the case here. On the other hand, a clear correlation was found in the present work between the $1/T_1$ and $1/T_2$ of tissues from the same brain, in agreement with (*20*).

The data shown prove that the form of the relaxation and contrast dispersions are characteristic for human brain white and gray matter. In fact, the contrast dispersion always has a similar shape when data from a gray/white matter tissue pair from one individual are compared. Although they may be subject to slight changes if more experimental data are collected and considered, data from Table 5 might be used as references for the description of the NMR characteristics of human brain gray and white matter. For purposes of comparison between gray and white matter, single data sets as given in Table 2 can also be used as in spite of the biological variability, the shapes of the relaxation and contrast dispersions are always the same; i.e., if in one individual the white matter dispersion is shifted upward relative to the average dispersion (probably due to a lower water content (*11, 27, 28*)), the gray matter curve is shifted upward as well.

DISCUSSION

Longitudinal Relaxation in White Matter

As mentioned above, the mathematical model (Eq. [1]) fits the data very well, but is not completely satisfying for white matter, due to the resulting negative baseline. The reason obviously lies in the strong high-field dispersion, not encountered for any other tissue except adipose, which, on the other hand, shows no dispersion at low fields. As neuroanatomy reports a very characteristic and uncommon structure and composition of white matter, it is very likely that these two findings are interconnected.

We have recently proposed an explanation of the uncommon relaxation dispersion of white matter on the basis of, on the one hand, neuroanatomical data and, on the other hand, NMR and ESR data obtained on membranes (*23*). In short, the explanation assumes that the water in the myelin sheath is influenced in its longitudinal relaxation by the membrane lipids, which by themselves are invisible to medical NMR techniques due to their short T_2. As the size of these molecules is much smaller than that of proteins, the resulting relaxation dispersion spreads to much higher frequencies. Whereas the exact mechanism and its interconnection with the "normal" relaxation pathway via proteins is still unclear, the analysis of the relaxation dispersion of white matter with a two-step function of the form

$$\frac{1}{T_1} = \frac{1}{T_{1,w}} + D + \frac{A_l}{1 + (f/f_{c,l})^{\beta_l'}} + \frac{A_h}{1 + (f/f_{c,h})^{\beta_h'}}, \qquad [6]$$

with the subscripts "l" and "h" indicating low-field and high-field dispersion, reveals one dispersion similar to that of gray matter and one resembling that of adipose tissue, with an inflection frequency corresponding to the molecular mobility found in phospholipid model systems. Moreover, the resulting baseline is positive and near the value for free water.

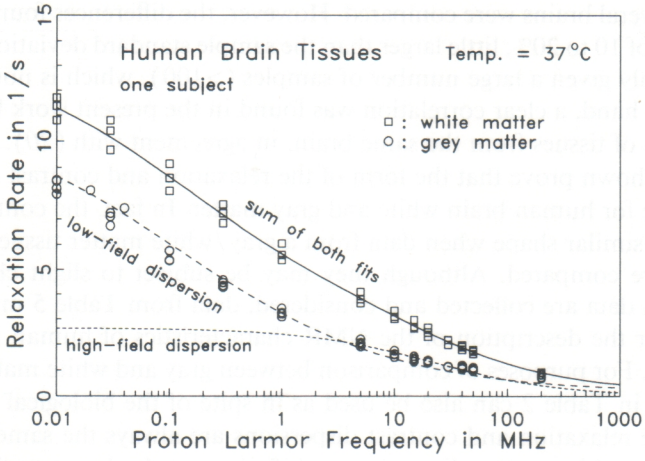

FIG. 9. Relaxation dispersions of all gray and white matter tissues from one brain (as in Fig. 7). The solid line is the result of curve fitting of all white matter data using Eq. [6] (two-step dispersion). The dashed lines indicate the contributions of each dispersion step. The low-field step also contains the baseline (D) and free water ($1/T_{1,w}$) contributions. The parameters of the two-step fit are given in Table 6.

The results of the application of Eq. [6] to white matter data are shown in Fig. 9 and Table 6. The results concerning curve fitting and T_1 contrast are not affected by these findings, as the shape of the sum curve virtually does not change. However, if extrapolations to very high or very low fields are required, the one- and the two-step dispersion models for white matter produce different results, of which the ones produced by the latter should be preferred. For example, the expected vanishing of the T_1 contrast at extremely high fields due to the fact that all tissue longitudinal relaxation rates approach that of water is predicted only by the two-step model.

Implications for Magnetic Resonance Imaging

The results described above have one obvious implication for MRI: due to the higher T_1 contrast, medium fields around 0.25 T can have an advantage over higher

TABLE 6

Fit Parameters for a Joint Treatment of All White Matter Samples from One Brain Obtained with Eq. [6], as Shown in Fig. 9

Parameter	Value
D (s^{-1})	−0.07
A_l (s^{-1})	11.00
$f_{c,l}$ (MHz)	0.135
β'_l	0.472
A_h (s^{-1})	2.64
$f_{c,h}$ (MHz)	21.42
β'_h	0.76

or lower fields for imaging of the CNS, as soon as a T_1 weighting is present in the imaging sequence and white matter is involved (this statement does not take into account the increase of signal-to-noise ratio with field). This is not valid for gray versus white matter only. Indeed most pathologiies will not have the high-field dispersion found for white matter, because

1. the pathological tissue or liquid may not contain myelin (e.g., tumors, inflammatory processes, hematomas), or
2. the pathology is associated with de- or dysmyelination, and thus the form of the T_1 contrast dispersion of pathologies versus white matter should be similar to that observed by us for gray versus white matter. Experiments performed on pathological samples support this assumption (*24*).

At medium-field strengths, the relative difference in T_1 between two tissues can be so high that sequences with very short TR can be used successfully, giving high image contrast. An example is shown in Fig. 10.

The graph shows, for different field strengths representing "low," "medium," and "high" fields, the absolute image contrast between gray and white matter for a spin–echo sequence, i.e.,

$$C_{abs} = I_{GM} - I_{WM}. \qquad [7]$$

The *absolute* contrast has been chosen here because it is related to the maximum obtainable signal and can be readily converted to a contrast-to-noise ratio by multiplication with the signal-to-noise ratio. The relative contrast, as used in Eq. [5], is more suitable to show tissue-inherent properties, which can be exploited in a suitable imaging sequence. If used for comparing signal intensities, the latter can produce misleading values (e.g., at extremely long TE and TR, for tissues with different T_2, a high relative contrast is obtained, but at a signal intensity approaching zero).

The respective signal intensities were calculated using the standard spin–echo sequence formula

$$I = \rho(1 - \exp(-\mathrm{TR}/T_1))\exp(-\mathrm{TE}/T_2) \qquad [8]$$

with ρ = "visible" proton density of the respective tissue, TR = repetition time of the sequence, TE = echo delay time of the sequence, and, $I_{max} = 1$.

The noise and the field dependence of the signal-to-noise ratio were neglected in this step. To eliminate the effect of varying T_1 on the sequence length at different fields, TR was expressed in units of T_1 of gray matter. T_2 was assumed to be constant with field, and "ideal" imaging conditions (ideal pulses, no effects of flow and diffusion) were also assumed. The tissue parameters from Table 2 were used for gray and white matter. Both longitudinal and transverse relaxation were assumed to be monoexponential. As the deviations of the real evolution of the magnetization from a monoexponential, as found in our experiments, are rather small, this simplification introduces only minor errors in the present calculations.

The graphs have identical shape for long TR and long TE, where the contrast is determined by ρ and T_2. However, for short TR and TE, i.e., heavy T_1 weighting, a negative contrast is obtained which is maximal for 10 MHz (Fig. 10b), the field at which the T_1 contrast between the two tissues is maximal, as shown in Fig. 5. With a

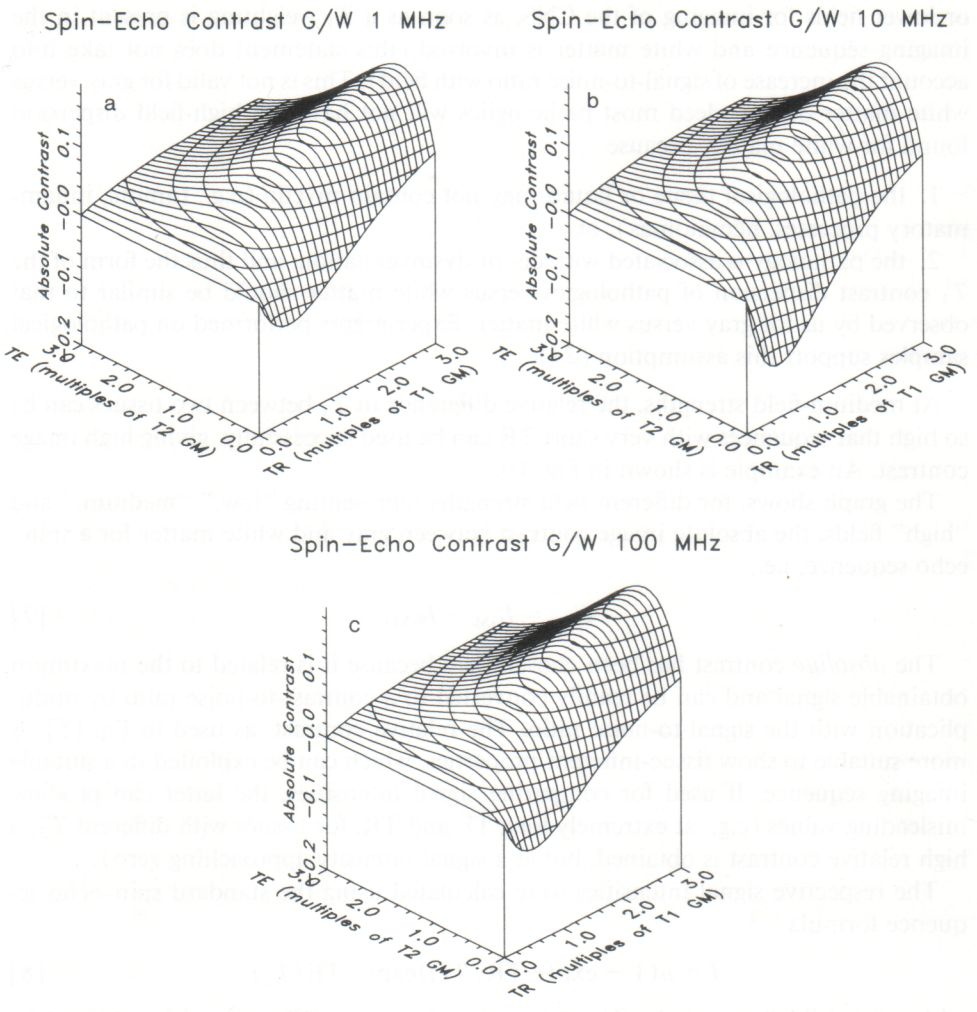

FIG. 10. Calculated absolute image contrast between gray and white matter for a spin–echo sequence, at various field strengths, obtained with Eqs. [7] and [8]. The tissue data were taken from Table 2. Contrast isocontours have a distance of 0.02 contrast units. (a) 1 MHz; (b) 10 MHz; (c) 100 MHz.

numerical value of −0.12 for TR = 0.5 T_1 (GM) and TE = 0 (i.e., a pure saturation-recovery sequence) the contrast is almost as high as that with long TR and long TE (maximum in the graphs ≈0.19), but with a much shorter imaging time and a better "visual contrast" due to the combination of high contrast and low signal intensity. The possible advantage of SR sequences with very short TR (combined with the disadvantage of reduced potential for multislice imaging) has already been pointed out in previous papers (*17, 29, 30*).

For gray and white matter, this effect is maximal at medium fields; for high and low fields, the corresponding negative contrast is less than half (−0.055). On the other hand, the obtainable S/N, according to Hoult and Lauterbur (*31*) and Hoult *et al.*

(*32*), for the human head should be roughly proportional to the field strength, yielding a factor of 10 between 10 and 100 MHz. This would result in an advantage in contrast-to-noise ratio of a factor of 4.6 for the high field. But as T_1 of gray matter at 100 MHz is almost double that at 10 MHz and T_1 of white matter is 2.4 times longer, the number of accumulations for the same imaging time can be more than double for the medium field, leaving a factor slightly higher than 3 of better C/N for a field 10 times higher, without taking into account problems specific to high fields, such as chemical shift artifacts.

This example shows the strong influence of the abnormal relaxation dispersion of white matter on image contrast. It also shows that the exact description of the relaxation dispersion of human brain gray and white matter offers the possibility to predict the image contrast produced by an imaging sequence at any desired field strength. Calculations such as those performed above could also be helpful in further clarifying the important question of "optimal field strength." Work in this field is currently in progress in our group (*33*).

CONCLUSIONS

Characteristic transverse decay data and longitudinal relaxation dispersions have been observed for the main constituents of human brain, i.e., gray and white matter. Each dispersion can adequately be described by a four-parameter function, the parameters of which are specific to the tissue type. White matter exhibits a dispersion not encountered in any other tissue, characterized by a strong dispersion at low and high fields. This is most probably caused by an additional relaxation process ocurring in myelin and involving the, themselves NMR-invisible, membrane lipids. Due to this fact, the relative difference in $1/T_1$ of gray and white matter shows a marked maximum at medium fields.

It is felt that consequences of this particular behavior will be important for neurological MRI, adding a new element to the sometimes controversial question of optimal field strength.

It has been shown that the obtained quantification of the relaxation behavior by curve fitting can be of valuable use in the prediction and optimization of image contrast in relation to hardware and imaging sequence parameters.

ACKNOWLEDGMENTS

The authors thank Drs. A. Lowenthal and D. Karcher for providing the tissue samples and Dr. L. Vander Elst and Mr. A. Roch for performing most of the 200-MHz measurements. Financial support was provided by the Commission of the European Communities (HWF) and Deutsche Forschungsgemeinschaft (PAR). The Relaxometer was acquired through a grant from the Fonds National de la Recherche Scientifique de Belgique.

REFERENCES

1. H. W. Fischer, Y. Van Haverbeke, P. A. Rinck, I. Schmitz-Feuerhake, and R. N. Muller, *Magn. Reson. Med.* **9,** 315 (1989).
2. Z. Györffy-Wagner, E. Eglund, E.-M. Larsson, A. Brun, S. Cronqvist, and B. Persson, *Acta Radiol. Diagn.* **27,** 115 (1986).
3. S. H. Koenig and R. D. Brown III, *in* "NMR Spectroscopy of Cells and Organisms" (R. K. Gupta, Ed.), Vol. II, p. 75, CRC Press, Boca Raton, FL, 1987.

4. P. T. BEALL, S. R. AMTEY, AND S. R. KASTURI, "NMR Data Handbook For Biomedical Applications," Pergamon, Elmsford, NY, 1984.
5. H. W. FISCHER, P. A. RINCK, A. LOWENTHAL, D. KARCHER, L. VANDER ELST, Y. VAN HAVERBEKE, AND R. N. MULLER, "9th European Experimental NMR Conference, Bad Aussee (A), May 1988," Book of Abstracts, p. 119, 1988.
6. H. W. FISCHER, P. A. RINCK, Y. VAN HAVERBEKE, I. SCHMITZ-FEUERHAKE, AND R. N. MULLER, *in* "Society of Magnetic Resonance in Medicine, 7th annual meeting, San Francisco, August 1988," Book of Abstracts, p. 234, 1988.
7. K. HALLENGA AND S. H. KOENIG, *Biochemistry* **15,** 4255 (1976).
8. S. CONTI, *Mol. Phys.* **59,** 3, 449 (1986).
9. S. H. KOENIG AND R. D. BROWN III, *Magn. Reson. Med.* **1,** 437 (1984).
10. S. H. KOENIG, R. D. BROWN III, D. ADAMS, D. EMERSON, AND C. G. HARRISON, *Invest. Radiol.* **2,** 77 (1984).
11. H. W. FISCHER, P. A. RINCK, AND R. N. MULLER, *in* "Tissue Characterization in MRI" (G. Bielke, H.-P. Higer, Eds.), Springer, Heidelberg, 1990.
12. P. A. BOTTOMLEY, T. H. FOSTER, R. E. ARGERSINGER, AND L. M. PFEIFER, *Med. Phys.* **11**(4), 425 (1984).
13. P. A. BOTTOMLEY, C. J. HARDY, R. E. ARGERSINGER, AND G. ALLEN-MOORE, *Med. Phys.* **14**(1), 1 (1987).
14. F. JAMES AND M. ROOS, *Comput. Phys. Commun.* **10,** 343 (1975).
15. A. FRANCOIS, L. VAN GERVEN, G. ATASSI, H. EISENDRATH, M. GIELEN, AND R. WILLEM, *Magn. Reson. Med.* **7,** 449 (1988).
16. W. T. NORTON AND W. CAMMER, *in* "Myelin" (P. Morell, Ed.), 2nd ed., p. 147, Plenum, New York, 1984.
17. F. W. WEHRLI, J. R. MCFALL, G. H. GLOVER, AND N. GRIGSBY, *Magn. Reson. Imaging* **2,** 3 (1984).
18. G. D. FULLERTON, *in* "Magnetic Resonance Imaging" (D. D. Stark, Ed.), p. 36, Mosby, St. Louis, 1988.
19. R. G. PARRISH, R. J. KURLAND, AND W. W. JANESE, *Science* **183,** 438 (1974).
20. E.-M. LARSSON, E. EGLUND, Z. GYÖRFFY-WAGNER, A. BRUN, S. CRONQVIST, AND B. PERSSON, *Acta Radiol. Diagn.* **27,** 231 (1986).
21. G. E. SANTYR, R. M. HENKELMAN, AND M. J. BRONSKILL, *J. Magn. Reson.* **79,** 28 (1987).
22. D. GRUCKER, Y. MAUSS, J. STEIBEL, P. POULET, AND J. CHAMBRON, *Biochim. Biophys. Acta* **887,** 249 (1986).
23. H. W. FISCHER, Y. VAN HAVERBEKE, I. SCHMITZ-FEUERHAKE, AND R. N. MULLER, *Magn. Reson. Med.* **9,** 441 (1989).
24. P. A. RINCK, H. W. FISCHER, L. VANDER ELST, Y. VAN HAVERBEKE, AND R. N. MULLER, *Radiology* **168,** 843 (1988).
25. P. A. RINCK, R. N. MULLER, AND H. W. FISCHER, *Fortschr. Roentgenstr.* **147**(2), 200 (1987).
26. J. M. ESCANYE, D. CANET, AND J. ROBERT, *Biochim. Biophys. Acta* **721,** 305 (1982).
27. E. EGLUND, A. BRUN, E.-M. LARSSON, Z. GYÖRFFY-WAGNER, AND B. PERSSON, *Acta Radiol. Diagn.* **27,** 653 (1986).
28. R. L. KAMMAN, K. G. GO, W. BROUWER, AND H. J. C. BERENDSEN, *Magn. Reson. Med.* **6,** 265 (1988).
29. P. R. MORAN, *Magn. Reson. Imaging* **2,** 17 (1984).
30. W. H. PERMAN, S. K. HILAL, H. E. SIMON, AND A. A. MAUDSLEY, *Magn. Reson. Imaging* **2,** 23 (1984).
31. D. I. HOULT AND P. C. LAUTERBUR, *J. Magn. Reson.* **34,** 425 (1979).
32. D. I. HOULT, C.-N. CHEN, AND V. J. SANK, *Magn. Reson. Med.* **3,** 730 (1986).
33. H. W. FISCHER, P. A. RINCK, Y. VAN HAVERBEKE, AND R. N. MULLER, Eighth Annual Meeting of the Society of Magnetic Resonance in Medicine, Amsterdam, August 1989, Book of Abstracts, p. 218.